Seamless Overtaking Maneuvers for Automated Driving: Integrated Motion Planning Based on Hybrid Model Predictive Control

Bo Leng, *Member, IEEE*, Ran Yu, Chengen Tu, Lu Xiong, Arno Eichberger, *Member, IEEE*, and Zhuoren Li, *Member, IEEE*

***Abstract*—Motion planning for automated vehicles faces critical challenges to achieve safe and efficient maneuvers. Classical modular motion planning, constrained by error propagation and inconsistent optimization objectives across different functional modules, often resulting in overly conservative or irrational overtaking maneuvers. To overcome these limitations, this article attempts to integrate discrete logic decision-making and continuous motion planning in a single optimal problem, and presents a hybrid model predictive control (HMPC)-based motion planner framework. In particular, a novel asymmetric risk fields considering human drivers' attention is incorporated to guide safe and timely intrinsic decision. The proposed framework eliminates the dependency on external semantic decision-making modules while ensuring efficient and safe maneuvers. Simulation and real vehicle test validate that the proposed HMPC framework is able to outperform the modular baseline, achieving safe and efficient overtaking maneuvers in an interpretable optimization approach.**

***Index Terms*—Artificial potential fields (APFs), automated vehicles, hybrid model predictive control, overtaking.**

I. Introduction

AUTONOMOUS vehicles (AVs), with their flexible decision-making capabilities and dynamic optimization mechanisms, are widely acknowledged for their potential to mitigate traffic accidents, enhance energy efficiency and occupant comfort, optimize traffic flow, and enable new forms of mobility [1]. In real-world driving environments, AVs must carry out complex overtaking maneuvers and make timely decisions to improve traffic efficiency while ensuring safety [2]. This presents significant challenges for motion planning systems of AVs. Generally, it is believed that existing motion planning algorithms can be broadly classified into two categories: modular scheme and integrated scheme.

The modular motion planning scheme typically consists of decision-making, trajectory planning, and motion control modules [3]. Based on the reference path from routing, decision-making selects the appropriate high-level driving behavior considering the perception results. Typical methods include decision trees [4], finite state machines [5], Markov processes [6], and game theory [7]. In accordance with the selected driving behavior, trajectory planning generates a collision-free spatio-temporal trajectory [8], commonly including: sample-based [9] and search-based approaches [10], which are computationally lightweight but limited by map resolution and dynamic adaptability; artificial potential field (APF) methods [11], which incorporate risk awareness by quantifying risks between the vehicle and its surrounding environment but struggle with local optima; and optimization-based methods [12], which formulate the planning problem as an optimization problem, minimizing performance metrics to obtain safe trajectories. Finally, motion control approach such as linear quadratic regulator (LQR) [13] and model predictive control (MPC) [14], are employed to compute desired control commands. Characterized by a clear logical structure, modular scheme based methods are easy to design and maintain. However, they are susceptible to issues such as information loss between modules, error propagation, and inconsistent optimization objectives, which can result in unexecuted or unreasonable motion, especially in dynamic scenarios such as overtaking maneuvers [2].

In addressing the issues inherent in the modular scheme, significant efforts have been dedicated to integrate the modules. Among them, MPC has gained prominence due to its ability to leverage predictive information and handle multiconstraint optimization, making it a predominant method for integrated motion planning [15]. Zuo et al. [16] apply MPC to both trajectory planning and tracking control, integrating them using

Received 11 August 2025; revised 30 November 2025; accepted 14 January 2026. This work was supported in part by the National Natural Science Foundation of China under Grant 52522219 and Grant 52325212, in part by SAIC Motor Corporation Limited under Grant 2023023, in part by the Fundamental Research Funds for the Central Universities under Grant 22120230311, and in part by the United Automotive Electronic Systems Company Ltd. under Grant NE-2003-10. *(Corresponding author: Zhuoren Li.)*

Bo Leng, Ran Yu, Chengen Tu, Lu Xiong, and Zhuoren Li are with the College of Automotive and Energy Engineering, Tongji University, Shanghai 201804, China (e-mail: lengbo@tongji.edu.cn; ranyu@tongji.edu.cn; 2133754@tongji.edu.cn; xiong_lu@tongji.edu.cn; 1911055@tongji.edu.cn).

Arno Eichberger is with the Institute of Automotive Engineering, Graz University of Technology, 8010 Graz, Austria (e-mail: arno.eichberger@tugraz.at).

Digital Object Identifier 10.1109/TIE.2026.3658697

the predicted state sequence as reference input. Hang et al. [17] develop a Stackelberg game-based decision-making model considering diverse driving behaviors, integrate it with MPC motion planning, and formulate a multiconstraint closed-loop optimization problem. However, existing MPC-based methods still require individual decision-making inputs to construct reference states or reference control inputs, which makes it difficult to seamlessly integrate optimal decision-making with motion planning, resulting in reduced flexibility and posing challenges when handling dynamic scenarios. Recent advances in learning-based methods, such as reinforcement learning [18] and imitation learning [19], have made significant progress in integrated motion planning, primarily by leveraging end-to-end (E2E) architectures to unify technical pipeline. However, these methods still lack clear and interpretable mechanisms to ensure safe and robust maneuvers of AVs.

Ensuring safety is paramount for real-world AV applications [20]. Classical MPC approaches directly use hard constraints to handle obstacles avoidance, which may result in solution failures or conservative behavior [16]. APF is widely used to reduce the collision risk with surrounding vehicles (SVs) through soft constraints or gradient solution [21]. Mainstream approaches combine MPC with APF to improve both safety and traffic efficiency [20], [21], [22], [23]. For instance, Zuo et al. [22] integrate lane decision-making into MPC using lane-associated APF as a cost term. Abdul et al. [23] assess the collision risk and optimize trajectory through MPC. However, most APF approaches neglect the nonuniform distribution of the driver's attention, which can lead to bias or overestimation in driving risk assessment, potentially resulting in either overly risky or overly conservative driving behavior decisions.

In this article, we propose an integrated motion planning framework based on hybrid model predictive control (HMPC) that incorporates logical constraints of lane-change behaviors and risk assessment to jointly solve the decision-making and motion planning problem in a unified optimal control problem, as shown in Fig. 1. This framework enables seamless information flow across modules and enforces consistent optimization objectives for decision-making, trajectory planning and motion control modules, ensuring globally consistent. Our previous work [24] established a basic HMPC structure for integrated motion planning. Building upon that foundation, this article further introduces an asymmetric risk field, which provides more informative guidance for intrinsic discrete lane-level behavior optimization. In addition, comprehensive experimental studies including simulation tests, dataset validations tests and real-world implementations are conducted to demonstrate the effectiveness of the proposed approach. The main contributions are as follows.

1) An HMPC-based integrated motion planning framework is proposed. It integrates discrete logic decision-making and continuous motion planning in a single optimal control problem without additional semantic decision module and seamlessly achieves efficient and safe driving.
2) An asymmetric risk field is introduced to guide intrinsic discrete behavior optimization. By considering the characteristics of the human driver's field of view and observational attention during driving, the risk field is dynamically adjusted for more reasonable representation.
3) The mixed logic dynamic system is formulated by incorporating discrete logical constraints into the optimization problem to adapt to discrete lane-level behavioral decisions, where both discrete lane change behavior, and continuous trajectory states and control command can be optimized simultaneously.
4) Comprehensive validation including MATLAB simulation, nuPlan benchmark validation and cloud-controlled real vehicle tests are performed to verify the algorithm's ability to identify overtaking opportunities and improve driving efficiency and safety. The results demonstrate the potential capability of integrating decision-making, trajectory planning and motion control in real AV tasks by an optimization scheme.

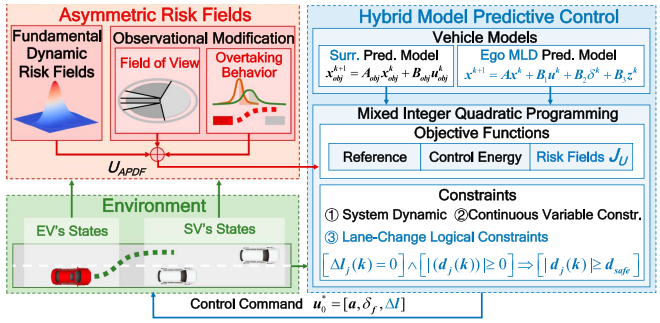

Fig. 1. Framework of our proposed method. Traffic dynamics are modeled to construct an asymmetric risk field, refined by drivers' field of view and overtaking behavior. The HMPC integrates this field into an MIQP-based framework, jointly generating continuous control commands and discrete lane-change decisions for seamless motion planning.

The remainder of this article is organized as follows: Section II presents the fundamentals of HMPC. Section III develops the asymmetric risk field framework incorporating surrounding vehicle dynamics and driver attention characteristics. Section IV formulates the motion planning problem through an HMPC perspective, detailing propositional logic derivation, MLD model conversion, constraint generation, and objective function design. Simulation analyses and experimental real-world validation are presented in Section V and VI, respectively. Finally, Section VII concludes the article.

II. Hybrid Model Predictive Control

A. MLD Model Construction

The mixed logic dynamic (MLD) system [25] formulates the hybrid system dynamics by encoding qualitative system knowledge and operational constraints through logical propositions. Leveraging Big-M modeling [26], it establishes formal equivalences between discrete Boolean variables and continuous variables, enabling unified mathematical representations via mixed-integer linear inequalities. Specifically, define $E = [x \leq 0]$ and introduce a Boolean variable $\delta \in \{0, 1\}$. When the proposition $E = true$, δ is set to 1. Using Big-M modeling, it can be derived that when the proposition $[x \leq 0] \Leftrightarrow [\delta = 1]$ is true, the variable

x satisfies the following linear inequalities:

$$\begin{cases} M\delta \le M - x \\ (\varepsilon - m)\delta \ge \varepsilon - x \end{cases} \tag{1}$$

where $\delta \in \mathbb{B}$, ε is a small positive value, M represents the upper bound of x, and m is the lower bound of x. Similar to the above process, discrete linear dynamical systems can be converted into a MLD model

$$\begin{aligned} x_{k+1} &= Ax_k + B_1u_k + B_2\delta_k + B_3z_k + B_5 \\ y_k &= Cx_k + D_1u_k + D_2\delta_k + D_3z_k + D_5 \\ E_2\delta_k + E_3z_k &\le E_4x_k + E_1u_k + E_5 \end{aligned} \tag{2}$$

where the state vector $x = [x_c, x_l]$, $x_c \in \mathbb{R}^{n_c}$ representing the continuous components and $x_l \in \{0,1\}^{n_l}$ are the discrete components of x, $n \triangleq n_c + n_l$ represents the dimension of the state variables. Similarly, the input u is divided as $[u_c, u_l] \in \mathbb{R}^{m_c} \times \{0,1\}^{m_l}$ and the output y is $[y_c, y_l] \in \mathbb{R}^{p_c} \times \{0,1\}^{p_l}$, m and p are the dimension of control variables and output variables, respectively. $z = x\delta$ is the auxiliary real variables.

B. HMPC Optimal Control Framework

For motion planning, we use discrete variables to encode behavioral semantics and continuous variables to control the vehicle's dynamics. By establishing the logical relationships between the decision semantics and vehicle dynamics, an MLD model is constructed and used as a predictive model for receding horizon optimization, resulting in an HMPC optimal control framework with objective function J

$$\begin{aligned} \min\ J &= \sum_{k=0}^{N-1} y_k^\top Q y_k + u_k^\top R u_k \\ \text{s.t. } x_{k+1} &= Ax_k + B_1u_k + B_2\delta_k + B_3z_k \\ y_k &= Cx_k + D_1u_k + D_2\delta_k + D_3z_k + D_5 \\ E_2\delta_k + E_3z_k &\le E_4x_k + E_1u_k + E_5 \\ x_{init} &= x_0 \end{aligned} \tag{3}$$

where $k \in \{0, \dots, N-1\}$ is prediction step, N is prediction horizon. If the objective function is quadratic and the weight matrix Q is semi-positive definite and R is positive definite, the HMPC optimization problem can be turned into a MIQP problem for solution

$$\begin{aligned} \min_\xi \quad & \frac{1}{2}\xi^\top H\xi + x_k^\top F\xi \\ \text{s.t.} \quad & G\xi \le W + Sx_k \end{aligned} \tag{4}$$

where G denotes the constraint matrix associated with the optimization variable ξ. S represents the matrix related to x_k. The optimized vector ξ consists of the control variable u_k, discrete auxiliary variable δ_k, and auxiliary real variable z_k

$$\xi = [\underbrace{u_0, \dots, u_{N-1}}_{\text{mixed-integer}}, \underbrace{\delta_0, \dots, \delta_{N-1}}_{\text{binary}}, \underbrace{z_0, \dots, z_{N-1}}_{\text{real}}]^\top. \tag{5}$$

III. Asymmetric Risk Fields

To guide intrinsic behavioral decision in the HMPC motion planning, a asymmetric risk field is designed considering two aspects: 1) the dynamic motion of SVs; and 2) the observational characteristics of SV drivers.

A. Fundamental Dynamic Risk Fields

Primarily, we use a 2-D Gaussian distribution to construct their static risk field

$$N(x_{ego} \mid \mu, \varepsilon) = \frac{A_{obs}}{2\pi\sqrt{|\varepsilon|}} e^{\left(-\frac{1}{2}(x_{ego}-\mu)^\top \varepsilon^{-1}(x_{ego}-\mu)\right)} \tag{6}$$

where N denotes the risk distribution function, A_{obs} represents the obstacle coefficient, $x_{ego} = (s, d)^\top$ is the EV's position in the Frenét coordinate system, and μ, ε the mean and covariance of the 2-D probability density function (PDF). During driving, changes in speed, acceleration, and heading angle affect driving risk. Based on these factors, the dynamic risk field $U_{pdf,k}$ generated by SVs is constructed as follows:

$$\begin{aligned} U_{pdf,k} &= w_1 \underbrace{C_1 e^{-0.5\times f_o^{(n)}}}_{N_1} + w_2 \underbrace{C_2 e^{-0.5\times g_o^{(n)}}}_{N_2} \\ C_1 &= \frac{A_{obs}}{2\pi\sqrt{\varepsilon_1}}, \quad C_2 = \frac{A_{obs}}{2\pi\sqrt{\varepsilon_2}} \\ {f_o}^{(n)} &= \mathbf{F}^\top {\varepsilon_1}^{-1}\mathbf{F}, \quad {g_o}^{(n)} = \mathbf{G}^\top {\varepsilon_2}^{-1}\mathbf{G} \\ \varepsilon_1 &= \begin{bmatrix} (S_{safe} - \Delta s_k^{(n)})^2 & 0 \\ 0 & (D_{safe} - \Delta d_k^{(n)})^2 \end{bmatrix} \\ \varepsilon_2 &= \begin{bmatrix} {S_{safe}}^2 & 0 \\ 0 & {D_{safe}}^2 \end{bmatrix}, \mathbf{F} = \begin{bmatrix} s_k - \hat{s}_k^{(n)} \\ d_k - \hat{d}_k^{(n)} \end{bmatrix} \\ \mathbf{G} &= \begin{bmatrix} s_k - (\hat{s}_k^{(n)} + \text{sign}(a_{k,s}^{(n)})\Delta s_k^{(n)}) \\ d_k - (\hat{d}_k^{(n)} + \text{sign}(a_{k,d}^{(n)})\Delta d_k^{(n)}) \end{bmatrix} \end{aligned} \tag{7}$$

where $w_1 \in [0.5, 1]$, $w_1 + w_2 = 1$, N_1 and N_2 are two independent 2-D Gaussian PDF, $U_{pdf,k}$ represents the dynamic risk fields of SVs at time k, w_1 and w_2 denote the weights of the two risk fields, and ε_1 and ε_2 are the covariance matrices. $\hat{s}_k^{(n)}$, $\hat{d}_k^{(n)}$, $a_{k,s}^{(n)}$, and $a_{k,d}^{(n)}$ represent the longitudinal displacement, lateral displacement, longitudinal acceleration, and lateral acceleration of the n-th obstacle, respectively. S_{safe} and D_{safe} denote the desired safe distances between the EV and SV in the longitudinal and lateral directions, respectively, which primarily determine the lengths of the major and minor axes of the risk field ellipse in the covariance matrix of the risk distribution function

$$\begin{cases} D_{safe} = w_d(D_{\min} + \Delta v_d^2/2a_c) \\ S_{safe} = w_s(S_{\min} + v_{ego}T_{safe} + \Delta v_s^2/2a_c) \end{cases} \tag{8}$$

where w_s and w_d represent the intensity of the safe distances. $S_{\min}$ and $D_{\min}$ denote the minimum safe distances between SVs and EV in the longitudinal and lateral directions, respectively. v_{ego} represents the EV's speed, T_{safe} is the safe time interval, Δv_s and Δv_d are the relative velocities between SVs and EV, and a_c denotes the acceleration of EV.

$\Delta s_k^{(n)}$ and $\Delta d_k^{(n)}$ represent the relative deviations of the risk field for the n-th obstacle vehicle at time k

$$\begin{cases} \Delta q_k^{(n)} = \frac{S_{b,q}}{e^{-p(|a_q|-0.5a_{q,\max})}}, & (q = s, d) \\ S_{b,q} = k_q S_q \end{cases} \tag{9}$$

where $S_{b,q}$ is the adjustable maximum deviation in each direction of the Frenét coordinate system, $a_{q,\max}$ denotes the maximum acceleration/deceleration of the SV, p is a positive coefficient and k_q is the mass coefficient. By combining N_1 and N_2, $U_{pdf,k}$ can consider both static geometric safety constraints and dynamic collision risks simultaneously, enabling the HMPC to plan more proactively and safely.

B. Observational Modification

Solely considering the vehicle's motion may overestimate the risk. In real-world driving scenarios, when the EV approaches or may influence SVs, SV driver typically take proactive avoidance actions, thereby reducing potential risk [28]. Therefore, we propose an observational risk field that integrates human driver attention patterns, leveraging an open-source eye-tracking dataset from Delft University of Technology [27]. This dataset captures drivers' visual attention allocation during normal driving and lane-changing maneuvers in simulated environments, offering insights into collision-avoidance behaviors.

1) Modification Based on Field of View (FOV): The FOV includes the forward view through the windshield and side windows and the side rear view through the exterior mirrors, but excludes the interior rear view mirror, which has minimal impact on the asymmetric risk field model. As demonstrated in Fig. 2(b), gaze points are more concentrated on the left, indicating a leftward attention bias. This reduces the risk when the EV is to the left of the SV, compared with when it is to the right. Based on the driver's FOV characteristics, we designed the asymmetric risk field as illustrated in Fig. 3. The relative distance d_{view} and angle θ_k of EV in the coordinate system of SV at the k-th moment are denoted as

$$\begin{aligned} d_{view} &= \sqrt{(x_{s,k} - (x_{o,k} + h_{x,k}))^2 + (y_{d,k} - (y_{o,k} + h_{y,k}))^2} \\ \theta_k &= \arctan 2(y_{d,k} - (y_{o,k} + h_{y,k}), x_{s,k} - (x_{o,k} + h_{x,k})) \end{aligned} \tag{10}$$

where $x_{o,k}$ and $y_{o,k}$ represent the SV's center of gravity (CG) in the coordinate system of SV and $h_{x,k}$ and $h_{y,k}$ represent SV's driver position in the coordinate system of SV. $x_{s,k}$ and $y_{d,k}$ represent EV's position in the coordinate system of SV. Determine if the EV is within the SV's visible sector based on d_{view} and θ_k, and represent the result as a boolean δ_{view}

$$\delta_{view} = \begin{cases} d_{view} \le l_{roi}, \theta_k \in [\theta_{fb}, \theta_{fe}] \\ d_{view} \le l_{roi} \sqrt{\left(1 + \frac{h_{y,k}}{w_{roi}}\right)\left(1 - \frac{h_{y,k}}{w_{roi}}\right)}, \theta_k \in [\theta_{lb}, \theta_{le}] \\ d_{view} \le l_{roi} \sqrt{\left(1 + \frac{w_{h,veh}}{w_{roi}}\right)\left(1 - \frac{w_{h,veh}}{w_{roi}}\right)}, \theta_k \in [\theta_{rb}, \theta_{re}] \end{cases}$$
$$view \in \{front, left, right\} \tag{11}$$

where θ_{fb} and θ_{fe} are the starting and ending angles of the forward visible sector, θ_{lb} and θ_{le} are for the left-side visible sector, θ_{rb} and θ_{re} are for the right-side visible sector, $view$ represents the distance, and $w_{h,veh}$ is the vehicle's half-width.

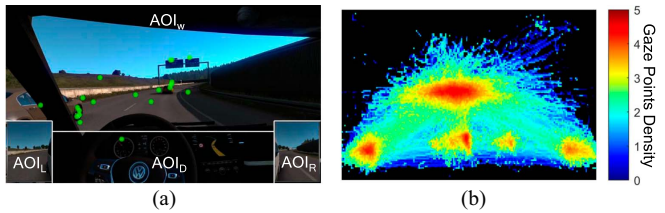

(a) (b)

Fig. 2. (a) Area of Interest (AOI): Gaze points (green) are divided into four AOIs: windshield $\mathrm{AOI_w}$, left and right rear-view mirrors $\mathrm{AOI_{L,R}}$, and dashboard $\mathrm{AOI_D}$, reflecting attention distribution. (b) Heat map of gaze points distribution, with color indicating gaze density on a logarithmic scale [27].

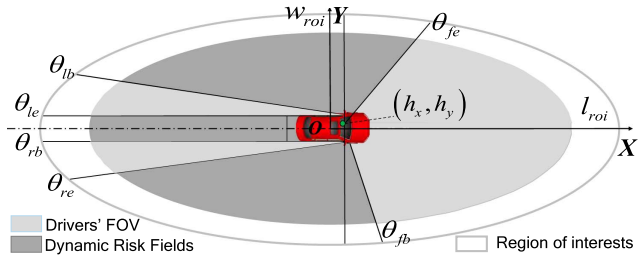

Fig. 3. Asymmetric risk field based on the driver's FOV. X and Y represent the coordinate axes of the SV's coordinate system, l_{roi} and w_{roi} indicating the driver's region of interests (ROI) in the longitudinal and lateral directions, which are set manually.

TABLE I
ATTENTION INTENSITY OF DIFFERENT AREAS OF INTEREST CALCULATED FROM GAZE POINT FREQUENCY

	$\mathrm{AOI_w}$	$\mathrm{AOI_L}$	$\mathrm{AOI_R}$	$\mathrm{AOI_D}$
Attention Intensity	0.58	0.21	0.12	0.09
Risk Intensity k_{view}	0.42	0.79	0.88	0.91

With the risk intensity of the ordinary risk field normalized to 1, the final risk intensity k_{view} is defined as 1 minus the corresponding attention intensity (as listed in Table I). When considering only the FOV, the risk field can be expressed as

$$U_{of,k} = k_{view} \cdot U_{pdf,k}, view \in \{front, left, right\}. \tag{12}$$

2) Modification Based on Overtaking Behavior: We statistically analyze the distribution of driver attention during overtaking maneuvers from the dataset, as shown in Fig. 4. The distributions approximately follow a normal distribution in both scenarios but differ significantly: when overtaken, the driver's attention is more focused before passing, while when overtaking, the attention peaks at overlap with higher variance. When SV is overtaking, assuming the longitudinal position of SV is x_{obs}, the driver's attention follows a normal distribution with a certain mean $\mu_{\text{overtake}} = x_{obs} - (l_{veh}/2 + l_{obs}/2)$ and variance $\sigma_{\text{overtake}} = (l_{veh}/2 + l_{obs}/2)/2$. Similarly, $\mu_{\text{overtaken}} = x_{obs}$ and $\sigma_{\text{overtaken}} = l_{veh}/2 + l_{obs}/2$ when SV is overtaken. Hence, the

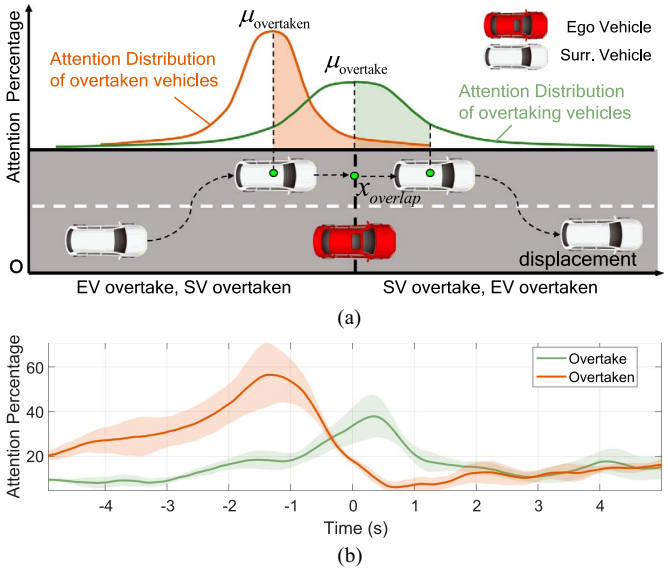

Fig. 4. (a) Attention distribution of drivers when overtaking and being overtaken. $x_{overlap}$ represents the position where the EV and SV overlap in the driving direction. (b) The curves of driver attention variations during overtaking maneuvers. Solid lines correspond to the mean and shaded regions correspond to 95% confidence interval.

attention intensity function of the two situations are

$$f_{att} = (2\pi\mu_{\text{type}}^2)^{-\frac{1}{2}} \exp\left[-\frac{(x-\mu_{\text{type}})}{2\sigma_{\text{type}}^2}\right] \tag{13}$$

where type $\in \{\text{overtake, overtaken}\}$, l_{veh} and l_{obs} are the length of EV and SV, respectively.

In this article, the risk from the SV to the EV is inversely proportional to the driver's attention of the SV. Thus, the attention intensity needs to be inverted and scaled. The attention normal distribution functions for both overtaking and being overtaken are flipped vertically around the x-axis, then shifted upwards according to the original peak, and finally normalized. The expression for the risk intensity function is as follows:

$$f_{risk} = \left(-f_{att} + \frac{1}{\sigma\sqrt{2\pi}}\right) \Big/ \frac{1}{\sigma\sqrt{2\pi}}. \tag{14}$$

Combined with (12), the final observational risk field is shown as follows:

$$U_{o,k} = k_{view} \cdot f_{risk} \cdot U_{pdf,k} \tag{15}$$

where $view \in \{front, left, right\}$. Finally, we can obtain the total asymmetric risk field

$$U_{APDF,k} = 0.5 \times (U_{pdf,k} + U_{o,k}). \tag{16}$$

IV. HMPC-Based Integrated Motion Planning

A. Vehicle Models

1) Hybrid Prediction Model of EV: The prediction model for HMPC is built upon a nonlinear single-track model. The model assumes no slip occurring between the tires and the road surface and is capable of predicting the vehicle's motion state with high accuracy when the lateral acceleration is lower than 0.4g [29],

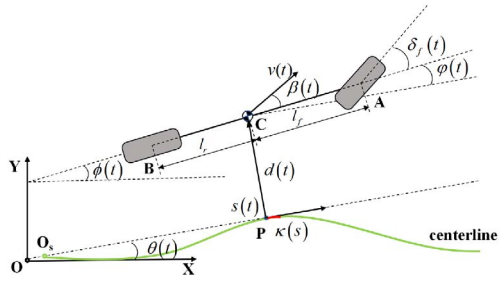

Fig. 5. Kinematic vehicle model in the Frenét coordinate system.

as illustrated in Fig. 5. Additionally, since vehicles typically do not experience sudden, excessive steering inputs during normal driving, small-angle approximations are generally applied to the slip and steering angles. Under this assumption, we transform the kinematic single-track model into the Frenét coordinate system

$$\begin{cases} \dot{s}(t) = \frac{v(t)}{1-\kappa(s)l(t)} \cos\left(\varphi(t) + \tan^{-1}\left(\frac{l_r \tan\delta_f(t)}{l_f+l_r}\right)\right) \\ \dot{d}(t) = v(t)\sin\left(\varphi(t) + \tan^{-1}\left(\frac{l_r \tan\delta_f(t)}{l_f+l_r}\right)\right) \\ \dot{\varphi}(t) = \frac{v(t)}{l_r}\sin\left(\tan^{-1}\left(\frac{l_r \tan\delta_f(t)}{l_f+l_r}\right)\right) - \kappa(s)\dot{s}(t) \\ \dot{v}(t) = a(t) \end{cases} \tag{17}$$

where s and d represent the longitudinal and lateral positions of the vehicle's CG in the Frenét coordinate system, ψ is the inertial heading angle, v is the vehicle's longitudinal velocity, l_f is the distance from the CG to the front axle, l_r is the distance from the CG to the rear axle, and κ denotes the curvature of the reference line at the point closest to the vehicle's current position. The front steering angle δ_f and longitudinal acceleration a are treated as the control inputs.

Since the lane is a integer variable and cannot be differentiated, it cannot directly integrated into the continuously vehicle kinematic model. Therefore, we discretize vehicle model using forward Euler, treating the lane as a discrete state variable. The discrete vehicle kinematic model is then augmented to derive the hybrid prediction model of the EV in the Frenét coordinate system, which is the MLD model of the EV

$$\begin{cases} s_{k+1} = s_k + \left(\frac{v_k}{1-\kappa_k d_k}\cos\left(\varphi_k + \arctan\left(\frac{l_r \tan\delta_{f,k}}{l_f+l_r}\right)\right)\right)T_s \\ d_{k+1} = d_k + \left(v_k \sin\left(\varphi_k + \arctan\left(\frac{l_r \tan\delta_{f,k}}{l_f+l_r}\right)\right)\right)T_s \\ \varphi_{k+1} = \varphi_k + \frac{v_k}{l_r}\sin\left(\arctan\left(\frac{l_r \tan\delta_{f,k}}{l_f+l_r}\right)\right)T_s \\ \qquad -\kappa_k \frac{v_k}{1-\kappa_k l_k}\cos\left(\varphi_k + \arctan\left(\frac{l_r \tan\delta_{f,k}}{l_f+l_r}\right)\right)T_s \\ v_{k+1} = v_k + a_k T_s \\ l_{k+1} = l_k + \Delta l_k. \end{cases} \tag{18}$$

The state vector of the system is defined as $\mathbf{x}_k = [s_k, d_k, \varphi_k, v_k, l_k]^\top$, and the control input vector of the system is $u_k = [\delta_{f,k}, a_k, \Delta l_k]^\top$. The lane variable l_{k+1} at the next moment is only related to the lane at the previous moment and the lane decision logic Δl_k.

2) Prediction Model of SVs: To avoid collisions and make timely lane change maneuvers, a prediction model of SVs is needed. In this article, a point mass kinematic model that assumes constant velocity is employed to describe the future motion of SVs, as expressed by the following equation:

$$\mathbf{x}_{obj,k+1} = \mathbf{A}_{obj}\mathbf{x}_{obj,k} + \mathbf{B}_{obj}\mathbf{u}_{obj,k} \tag{19}$$
$$\mathbf{A}_{obj} = \begin{bmatrix} 1 & 0 & 0 & T & 0 \\ 0 & 1 & 0 & 0 & 0 \\ 0 & 0 & 1 & 0 & 0 \\ 0 & 0 & 0 & 1 & 0 \\ 0 & 0 & 0 & 0 & 1 \end{bmatrix}, \mathbf{B}_{obj} = \begin{bmatrix} 0 & 0 \\ 0 & 0 \\ 0 & 0 \\ 0 & 0 \\ 0 & 0 \end{bmatrix}$$

where $\mathbf{x}_{obj,k} = [s_{obj,k}, d_{obj,k}, \varphi_{obj,k}, v_{obj,k}, l_{obj,k}]^\top$ represents the state of the dynamic obstacle vehicle, including the longitudinal position $s_{obj,k}$, lateral position $d_{obj,k}$, heading angle $\varphi_{obj,k}$, velocity $v_{obj,k}$, and current lane $l_{obj,k}$, input vector $\mathbf{u}_{obj,k} = [\delta_{obj,f}, a_{obj}]$.

B. Constraints

The constraints are mainly composed of three parts: logic constraints, system dynamics equality constraints, and state and control variable constraints. The system dynamics equality constraints are derived from (18). The bounds of the variables are defined depend on road boundaries, safety

$$\begin{aligned} &|\varphi_k| \le \varphi_{limit}, 0 \le v_k \le v_{limit} \\ &|\delta_{f,k}| \le \delta_{f,limit}, a_{dec,limit} \le a_k \le a_{acc,limit}. \end{aligned} \tag{20}$$

Before introducing the logic constraints, we define the concept of safe distance d_{safe}. d_{safe} ensures that during overtaking, the EV will not collide with preceding or subsequent vehicle in the target lane, as illustrated in Fig. 6. Safe distance is calculated based on the vehicle speed, time to collision (TTC), and maximum deceleration

$$d_{safe}(k) = v_{rear} \times \mathrm{TTC}_{rear} + d_c^{rear}(k) - d_c^{front}(k)$$
$$\begin{cases} d_c^u(k) = v_u(k) \times T_s \times n_u(k) \\ -v_r^u(k) \times T_s \times \frac{n_u(k)(n_u(k)+1)}{2} \\ v_r^u(k) = b_{\max} \times T_s \\ n_u(k) = v_u(k)/v_r^u(k) \\ u = [front, rear] \end{cases} \tag{21}$$

where $u = [front, rear]$ indicate that vehicle u is the front or rear vehicle when calculating d_{safe}. If d_{safe} between the EV and the leader vehicle is calculated, then $front =$ leader vehicle, $rear =$ EV. $\mathrm{TTC}_{\mathrm{rear}}$ is the TTC of the rear vehicle, v_u is the velocity of the vehicle u, T_s is the sample time of the system and $b_{\max}$ is the maximum deceleration.

Based on the safe distance, we construct the logical constraints for the HMPC. We consider vehicles driving in a multilane environment $\mathcal{L} = \{1, 2, \ldots, L\}$, where L is the total number of lanes. Treat the EV as controlled plant, continuous variable as acceleration a and discrete variable as lane l. To ensure the EV operates safely in this environment, it is specified that the vehicle can only switch to an adjacent lane when changing lanes, and cannot change to a non-adjacent lane. Additionally, the speed must remain within the limits

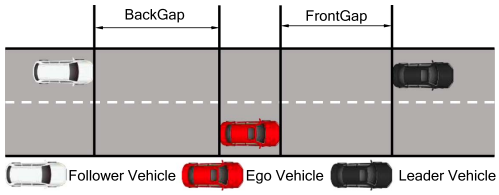

Fig. 6. Safe distance for vehicle lane changes.

$$\begin{aligned} &0 \le v(k) \le v_{\max}, \forall k \in T_p \\ &\max\{1, l(k)-1\} \le l(k+1) \le \min\{L, l(k)+1\}, \forall k \in T_p. \end{aligned} \tag{22}$$

Meanwhile, the longitudinal and lateral distances between the EV and the j-th SV are defined as follows:

$$\begin{aligned} d_j(k+1) &= d_j(k) + T_s(v_j(k) - v(k)), \forall k \in T_p \\ \Delta l_j(k) &= l_j(k) - l(k) \in \{-L+1, L-1\}, \forall k \in T_p \end{aligned} \tag{23}$$

where $T_p = \{1, 2, \ldots, N_p\}$ is the prediction horizon.

Based on the above definitions, the propositional logic for the EV's lane-changing decision is designed as follows: When EV and SV are in the same lane, the distance between the two vehicles must be greater than the safe distance d_{safe}

$$\underbrace{[\Delta l_j(k) = 0]}_{(A)} \wedge \underbrace{[|(d_j(k))| \ge 0]}_{(B)} \Rightarrow \underbrace{[|d_j(k)| \ge d_{safe}]}_{(C)}. \tag{24}$$

Based on the basic rules of logical conversion, (24) can be transformed into mixed integer inequalities. The details are provided in the appendix.

C. Objective Functions

The optimization objectives of all modules are integrated into a unified objective function.

1) Decision-Making Relative Objective: To enable lane-aware lateral displacement adjustment, the desired lateral distance is defined as the product of the target lane index l_k and the lateral distance w between the current and target lane centerlines. Therefore, the lateral distance objective function $J_{d,k}$ and the lane objective function $J_{l,k}$ at the k-th time step can be expressed as

$$J_{d,k} = q_d(d_k - l_k w)^2, J_{l,k} = q_l(l_k - l_{ref,k})^2 \tag{25}$$

where $q_{(\cdot)}$ is the weight of corresponding term. $l_{ref,k}$ is the reference lane index, which is set to 0 by default and can be replaced with the corresponding value when there is external semantic decision input.

Additionally, the asymmetric risk field is included as part of the optimization objective $J_{U,k} = \sum_1^{N_j} U_{APDF,k}$. The risk fields of N_j SVs are summed to represent the overall environmental risk, which guides the vehicle's lane change decisions.

2) Planning Relative Objective: It is primarily used to guide the state transitions of the vehicle during motion planning, with a focus on speed and heading angle

$$J_{\varphi,k} = q_\varphi \varphi_k^2, J_{v,k} = q_v (v_k - v_{ref,k})^2 \tag{26}$$

where $v_{ref,k}$ is the expected speed. Typically, the expected speed is associated with the curvature of the reference path. The greater the curvature, the more restricted the vehicle's acceleration, resulting in a lower expected speed.

3) Control Relative Objective: Since small variations in the system's control inputs help ensure the safety of the automated vehicle during its motion, the objective functions for the steering angle and acceleration are defined as follows:

$$J_{\delta_f,k} = r_{\delta_f} \delta_{f,k}^2, J_{a,k} = r_a a_k^2 \tag{27}$$

where r_{δ_f} and r_a are the weight of corresponding term.

D. HMPC Problem Formulation and Solution

The full optimal control problem (OCP) for the integrated motion planner is formulated as follows:

$$\begin{aligned} J &= \sum_{k=1}^{N_p} \|\mathbf{x}_k - \mathbf{x}_{ref}\|_{\mathbf{Q}}^2 + \sum_{k=0}^{N_p-1} \|\mathbf{u}_k\|_{\mathbf{R}}^2 + J_U \\ &= \sum_{k=1}^{N_p} (J_{d,k} + J_{\varphi,k} + J_{v,k} + J_{l,k}) \\ &\quad + \sum_{k=0}^{N_p-1} \left(J_{\delta_f,k} + J_{a,k}\right) + J_U \end{aligned} \tag{28}$$

$$\text{s.t.} \begin{cases} \text{System dynamic} : (18) \\ \text{Continuous variable constraints} : (20), (22), (23) \\ \text{Logical constraints} : (24) \\ \mathbf{x}_k \in \mathbf{\Xi}, \forall k \in \{1, 2, \ldots, N_p\} \\ \mathbf{u}_k \in \mathbf{U}, \forall k \in \{0, 1, \ldots, N_p - 1\} \end{cases} \tag{29}$$

where $\mathbf{\Xi}$ and $\mathbf{U}$ represent the feasible sets of system states and control inputs, respectively. $\mathbf{Q}$ and $\mathbf{R}$ are the positive semi-definite weight matrices for the system state vector and control input vector, respectively. The nonlinear optimization problem will be solved using the Gurobi solver.

V. Simulation Verification

A. Numerical Simulation

To validate that the automated vehicle can safely perform overtaking maneuvers without compromising traffic efficiency, we use MATLAB to set up two numerical simulation. The scenario involves overtaking on a straight road with multiple SVs. The lane width $w = 3$, road length $l_{road} = 500$, and all vehicles are modeled with the same rectangular shape. The vehicle parameters include $l_{veh} = 2.5$, $w_{veh} = 1.5$, and $l_f = 1.5, l_r = 1.0$. The rightmost lane is defined as lane 0, with lane numbers increasing from right to left. The coordinate axis is aligned with the centerline of lane 0, and the axis originates from the starting point of the road for lane 0, as depicted in Fig. 7. The set of simulation parameters is listed in Table II. In the following, we compare the proposed HMPC method with and without semantic decision-making, and the classical MPC motion planning method with a hierarchical architecture: the upper layer of classical MPC relies on the aforementioned safe distance for semantic decision-making, while the lower layer integrates planning and control, directly outputting control commands. For brevity, we refer to these methods as HMPC and MPC.

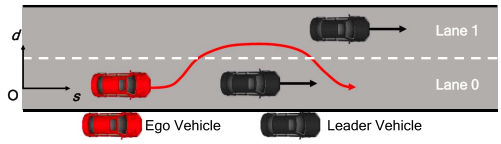

Fig. 7. Lane change scenario considered in the simulations.

TABLE II
Set of Simulation Parameters

Parameter	Description	Value	Unit
T_s	Sampling time	0.1	s
N_p	Prediction horizon	10	-
N_j	Number of surrounding vehicles	2	-
$\mathbf{Q}$	Output weight	diag(10,1,5,1)	-
$\mathbf{R}$	Input weight	diag(1,5,1,...,0)	-
TTC	Time to collision	1	s
b_{max}	Maximum deceleration	4	m/s^2
$\underline{v}, \overline{v}$	Velocity bounds	$[0, 35]$	m/s
$\underline{a}, \overline{a}$	Acceleration bounds	$[-4, 4]$	m/s^2
$\underline{l}, \overline{l}$	Lane bounds	$[0, 1]$	-
$\underline{\delta_f}, \overline{\delta_f}$	Steering wheel bounds	$[-0.5, 0.5]$	rad
w_1, w_2	Weight of Dynamic risk field	0.7, 0.3	-
θ_{fb}, θ_{fe}	Angle of driver's FOV (front)	$[-80°, 60°]$	deg
θ_{lb}, θ_{le}	Angle of driver's FOV (left)	$[161°, 177°]$	deg
θ_{rb}, θ_{re}	Angle of driver's FOV (right)	$[-177°, -166°]$	deg

Note: $\theta_{(\cdot)}$ are designed based on Chinese standard [30].

In the first case, EV is initialized with $\mathbf{x}_0 = [0, 0, 0, 28, 0]^\top$ and is required to maintain its desired longitudinal velocity of 28 m/s. Two SVs are considered in this configuration: SV1 is driving in lane 0 at a lower speed $\mathbf{x}_0^{SV1} = [100, 0, 0, 15, 0]^\top$, while SV2 is driving in front of EV and SV1 in lane 1 with a higher speed than SV1 but also a lower speed than EV $\mathbf{x}_0^{SV2} = [130, 3, 0, 21, 1]^\top$. The EV needs to pass through the gap and overtake the slower vehicle in front in order to improve its traffic efficiency. The test results are illustrated in Fig. 8. When utilizing pure HMPC, the EV first maintains its current lane and performs a timely lane-change maneuver when blocked by SV1 (below). Meanwhile, by considering both decision-making and motion planning simultaneously, HMPC effectively identifies the optimal overtaking opportunity, completing the overtaking maneuver with sufficient space between SV2 (above) and SV1, without losing speed. MPC with semantic decision-making shows a contrasting behavior. Since its decision module operates independently, it may not determine the optimal overtaking timing, causing the vehicle to slow down and follow SV2 for a period before completing the overtaking maneuver. Moreover,

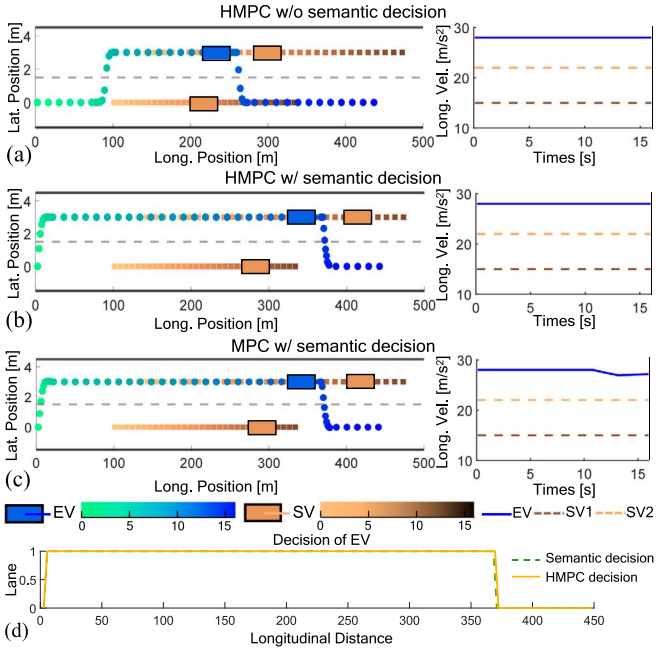

Fig. 8. Results of simulation experiment case 1. (a)–(c) Vehicle trajectory during an overtaking maneuver with key moments indicated and corresponding longitudinal speed profile. (d) Comparison between the semantic decision and the HMPC decision (with the semantic decision).

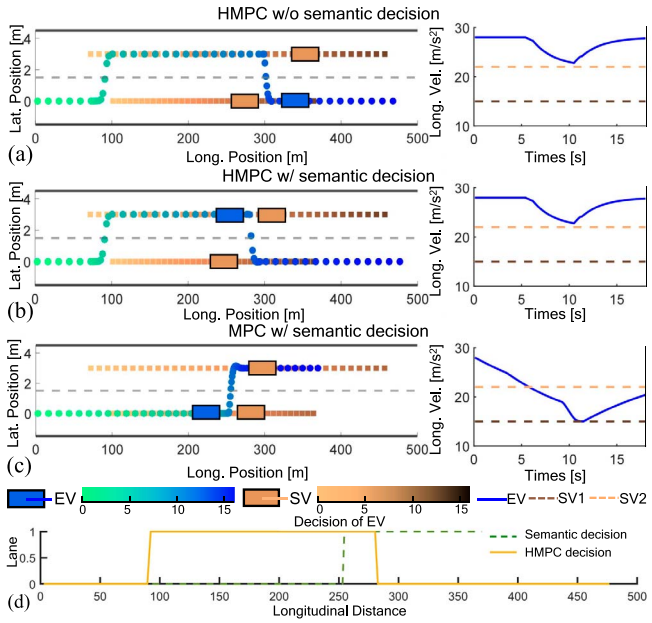

Fig. 9. Results of simulation experiment case 2. (a)–(c) Vehicle trajectory during an overtaking maneuver with key moments indicated and corresponding longitudinal speed profile. (d) Comparison between the semantic decision and the HMPC decision (with the semantic decision).

as discussed in Section IV-C, HMPC is capable of integrating external semantic decision-making to reschedule motion planning. When using the same semantic decision as MPC, HMPC did not immediately execute the lane change as suggested by the semantic decision. Instead, it re-optimized the timing of the lane change, enabling the vehicle to complete the maneuver without losing speed.

The scenario in case 2 is similar to that in case 1, but more complex. In case 2, SV2 $\mathbf{x}_0^{SV2} = [70, 3, 0, 21, 1]^\top$ lags behind SV1 $\mathbf{x}_0^{SV1} = [100, 0, 0, 16, 0]^\top$ and gradually overtakes it. As a result, as SV1 moves slowly and SV2 approaches from the adjacent lane behind, the EV $\mathbf{x}_0 = [0, 0, 0, 28, 0]^\top$ must decide between slowing down and following SV1 or changing lanes to overtake. Test results demonstrating these results are presented in Fig. 9. When using pure HMPC, the EV first detects the potential obstruction by SV1 and applies a lane change maneuver to follow SV2 to achieve a higher speed. Once a safe gap between SV1 and SV2 is confirmed, the EV seamlessly completes the overtaking maneuver. In contrast, hierarchical MPC prioritizes maintaining safe distances, delaying lane changes until a sufficient gap between SV1 and SV2 is available. This causes the EV to slow down and miss the optimal lane change timing, resulting in a loss of speed. In this case, since the semantic decision in MPC cannot effectively capture the optimal lane change timing, HMPC (with semantic decision) makes a different choice that better minimizes the EV's speed loss, as shown in Fig. 8(d). The final result is similar to pure HMPC, indicating that the proposed approach not only optimizes external semantic decisions comprehensively but also demonstrates good robustness.

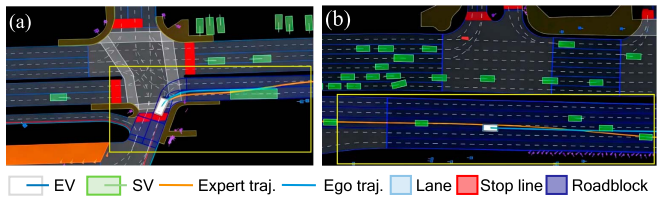

Fig. 10. (a) Merging and overtaking. The EV needs to perform a right-turn maneuver to merge into the main road, and then overtake the leading large vehicle. (b) Multilane overtaking. The EV need to execute a right lane-change maneuver and then follow the leader vehicle.

B. Validation on NuPlan Benchmark

In view of the simplicity and fixed nature of the scenarios in Section V-A, which renders it challenging to simulate the complex variations of traffic flow in real-world scenarios, we conduct more comprehensive testing based on nuPlan [31], a large-scale closed-loop planning benchmark for autonomous driving , as shown in Fig. 10.

In our simulation setup, SVs are controlled using a log-replay mode with no reaction (NR) to the EV. For algorithms that generate trajectories without direct control commands, we employ an LQR controller for tracking. EV's states are then updated using a kinematic single-track model. We choose the hierarchical MPC, as described in Section V-A, and the end-to-end imitation learning (IL)-based planning algorithm PlanTF [32] (the official baseline in nuPlan) as the baseline. PlanTF is trained on 150 000 scenarios from the nuPlan dataset, using the vehicle's trajectory over the past 3 seconds as input to generate the trajectory for the next 8 s.

TABLE III
EVALUATION METRICS OF PLANNING ALGORITHM

Metric Name	Description
NR closed-loop score (NR-CLS)	Evaluates the algorithm's overall performance in NR closed-loop scenarios.
Average displacement error (ADE)	Average L2 distance deviation between the EV's trajectory and the expert trajectory.
Derivable area compliance (DAC)	Whether EV stays in drivable area.
Derivable direction compliance (DDC)	Whether EV moves along the defined driving direction in the time domain.
Comfort	Whether EV's lateral/longitudinal acceleration meets the threshold.
Progress along route ratio (PRR)	EV's progress along expert trajectory.
No at-fault collisions (NAC)	Whether EV has any at-fault collisions.
Speed limit compliance (SLC)	Whether EV follows the map speed limit.

Note: All metric scores are normalized to the [0–1] range using official thresholds.

TABLE IV
SIMULATION RESULTS OF THE TEST-LC DATASET

Methods	NR-CLS (↑)	DAC (↑)	DDC (↑)	Comf. (↑)	PRR (↑)	NAC (↑)	SLC (↑)	SR (↑)	ACT(ms) (↓)
MPC	0.882	0.833	0.955	0.812	0.791	0.912	0.952	74/100	**43**
PlanTF	0.633	**0.918**	0.932	**0.863**	0.709	0.809	0.940	56/100	152
HMPC	**0.911**	0.817	**0.958**	0.823	**0.835**	**0.913**	**0.954**	**87/100**	77

Note: SR stands for the success rate, and ACT is the average computation time per step. The prediction horizon N_p for both HMPC and MPC is set to 20. Bold entries indicate the best performance.

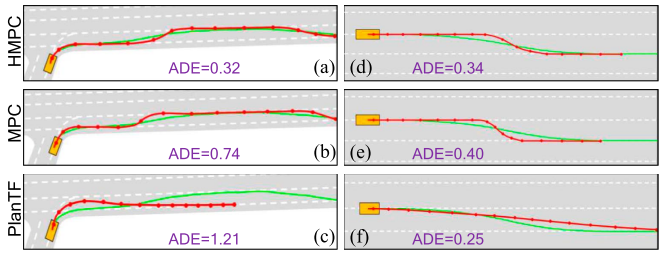

Fig. 11. Trajectory visualization of nuPlan cases. Green lines represent the expert trajectory, while red lines indicate the EV's trajectory.

TABLE V
SIMULATION RESULTS OF THE TEST-RANDOM AND TEST-HARD

Test Type	Methods	NR-CLS (↑)	DAC (↑)	DDC (↑)	Comf. (↑)	PRR (↑)	NAC (↑)	SLC (↑)
random	MPC	0.891	0.833	0.955	0.832	0.781	**0.912**	0.983
	PlanTF	0.848	**0.938**	**0.985**	0.803	**0.879**	0.890	0.960
	HMPC	**0.901**	0.817	0.954	**0.833**	0.812	0.903	**0.985**
hard	MPC	0.676	0.781	0.909	**0.821**	0.677	0.854	**0.959**
	PlanTF	**0.757**	**0.903**	**0.953**	0.772	**0.818**	0.835	0.923
	HMPC	0.690	0.744	0.908	0.816	0.693	**0.865**	0.954

Note: Bold entries indicate the best performance.

We evaluate the algorithm in both targeted lane-change and general multiscenario tests to quantify not only HMPC's performance gains in lane-changing over baselines, as well as its generalization capacity. The official nuPlan metrics is used for evaluation, and the details are listed in Table III.

1) Test on Lane Change Scenario: We selected 100 lane-change scenarios from the nuPlan dataset to construct the *Test-LC* set, and the evaluation results are shown in Table IV. HMPC outperforms or matches the other algorithms across multiple metrics, with its NR-CLS being 3.28% and 43.9% higher than MPC and PlanTF, respectively. HMPC accounts for the driver's FOV and dynamic attention, not merely the safety distance, resulting in more human-like behavior and a 5.22% improvement in PRR over MPC. The integrated planning framework also reduces inter-module error, facilitating smoother maneuvers and more successful overtaking in lane changes. PlanTF performs poorly in these scenarios, as it fails to capture the underlying causal logic of lane-changing through IL, resulting in overly conservative lane-keeping behavior. The scarcity of lane-change instances in the training data further hinders effective learning of such maneuvers. Despite a higher computational consumption than MPC due to solving a MIQP problem integrated with a risk field, HMPC's average computation time (ACT) remains under 100 ms, meeting real-time requirements.

We further analyze two typical scenarios. As shown in Fig. 11, HMPC achieves a smaller ADE than MPC in both cases, with lane-change timing closer to the expert trajectory. MPC relies solely on safety distance to determine lane changes, resulting in suboptimal timing and abrupt maneuvers. In the first case, PlanTF fails to perform the lane change and exhibit an overly large turning radius. In the second case, while it has the lowest ADE, the long lane-change distance still poses potential risks. This is because PlanTF lacks a causal decision model and depends on historical motion inputs, thus favoring the maintenance of the current driving state.

2) Test on Multiscenario: We selected seven types of scenario related overtaking from the nuPlan for evaluation, including *changing lane*, *high magnitude speed*, *near multiple vehicles*, *high lateral acceleration*, *following lane with lead*, *low magnitude speed*, and *behind long vehicle*. To comprehensively assess HMPC's generalization ability across diverse driving conditions and its adaptability to long-tail scenarios, we constructed two types of test sets: 1) *Test-random*: a fixed test set composed of 20 randomly sampled scenarios from the seven categories above; and 2) *Test-hard*: A high-difficulty set is formed by selecting the 20 most challenging scenarios from 100 initial cases per type, as identified by the poor performance of the state-of-the-art rule-based planner [PDM-Closed [33]].

As illustrated in Table V, HMPC achieved improvements of 1.12% and 6.25% over MPC and PlanTF, respectively, on the NR-CLS within the *Test-random*. By incorporating driver behavior modeling, HMPC achieves planning closer to expert behavior and a 3.97% higher PRR than MPC. However, as its risk field parameters are calibrated from highway data, HMPC suffers from model mismatch in diverse scenarios, leading to weaker generalization. Consequently, its DAC and NAC metric are reduced by 1.90% and 1.04%, respectively compared with MPC. Although PlanTF excels in PRR by exhibiting human-like behavior, its lack of formalized safety constraints in the end-to-end trajectory results in suboptimal NAC performance.

On the *Test-hard* benchmark, the NR-CLS of HMPC and MPC decreased by 23.4% and 24.1%, respectively, compared with the *Test-random* benchmark. The performance drop is

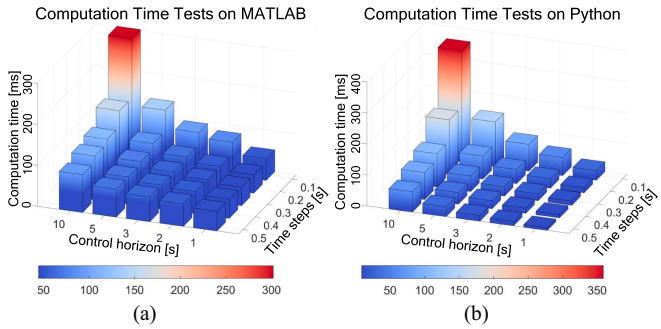

Fig. 12. Computation time of various control horizons and time steps. The tests in nuPlan and the real-world are both based on Python.

primarily due to the complex traffic behaviors in long-tail scenarios, where the optimization objectives and constraints are highly coupled, making it difficult for rule-based methods to solve. In contrast, PlanTF demonstrates better generalization ability, but its lack of safety constraints results in NAC that are still 3.40% and 2.12% lower than those of HMPC and MPC, respectively. Future work will explore physics-informed learning algorithms to balance generalization ability while satisfying safety constraints.

C. Sensitivity Analysis on Computation Time

We further perform a sensitivity analysis on the algorithm's computation time. The MATLAB and nuPlan simulations were conducted on an Intel i7-12700H CPU at 2.3 GHz, with each simulation repeated five times under random initial conditions. The real-world tests (see Section VI) employ an Intel i9-9900K CPU at 3.6 GHz. As shown in Fig. 12, the computation time increases exponentially with a shorter time step and a longer control horizon, indicating the need for a tradeoff between temporal resolution and prediction range during deployment. Therefore, we selected $T_s = 0.1s$ and $N_p = 10$ to balance computational burden and performance. Table VI shows the computation time statistics for different platforms and numbers of SVs. In all configurations, the average computation time for HMPC remains below 100 ms, with the worst case slightly exceeding 100 ms, meeting the real-time motion planning requirement of a 10 Hz update frequency. To further enhance scalability and real-time performance in more complex environments, future work will focus on reducing the computational complexity of the algorithm. In addition, implementing HMPC on a dedicated hardware platform is expected to provide further computational gains.

VI. Test on Real-World Roads

Based on our previous work [34], we validate our algorithm using the cloud-controlled testing framework built at Tongji University's Smart Networked Automobile Testing and Evaluation Base. As illustrated in Fig. 13, the experiment integrates an experiment vehicle (ExV), which act as the EV, with an cloud-based intelligent connected vehicle control system for real-world validation. The cloud-based host simultaneously controls

TABLE VI
Computation Time Statistics on Different Platform

Test Platform	MATLAB Implementation	nuPlan Benchmark	Real-World Vehicle
Avg Comp. time (ms)	53.15	31.71	50.74
Min Comp. time (ms)	45.81	27.96	32.02
Max Comp. time (ms)	103.7	62.26	71.11

Note: The prediction horizon N_p is set to 10 and sampling time $T_s = 0.1s$.

Fig. 13. (a) Experiment vehicle. (b) Cloud-controlled simulated vehicle.

Fig. 14. (a) Two-lane overtaking scenario. (b) Three-lane overtaking scenario.

both the ExV and cloud-controlled simulated vehicles (CSVs), where motion planning algorithms are deployed. The CSVs act as SVs, transmitting real-time localization data to the cloud host to provide ground-truth positioning for the ExV. After motion planning is employed in the cloud, control commands are sent to the ExV via the message queuing telemetry transport (MQTT) protocol to enable vehicle control. The ExV features a drive-by-wire chassis system, controlled via CAN bus commands. The ExV is also equipped with a high-precision integrated positioning system for accurate pose estimation, along with five LiDARs and three cameras to detect and predict static and dynamic obstacles. During testing, real-time chassis pose and status data were uploaded to the cloud host via a 5G communication module, while control commands were transmitted back through the same channel. The vehicle control unit (VCU) executed steering, acceleration, and braking actions via CAN bus communication, ensuring closed-loop control.

A. Case 1: Two-Lane Overtaking Scenario

In the first case, the EV begins with an initial velocity of 0 km/h and gradually accelerates to the desired velocity of 50 km/h. The leader vehicle SV1 is positioned 50 meters ahead in the same lane as the EV, moving straight at 16 km/h, while SV2 is situated 45 meters ahead in the left adjacent lane, traveling straight at 10 km/h. The designed scenario is depicted in Fig. 14(a). As shown in Fig. 15, the EV accelerates for the first

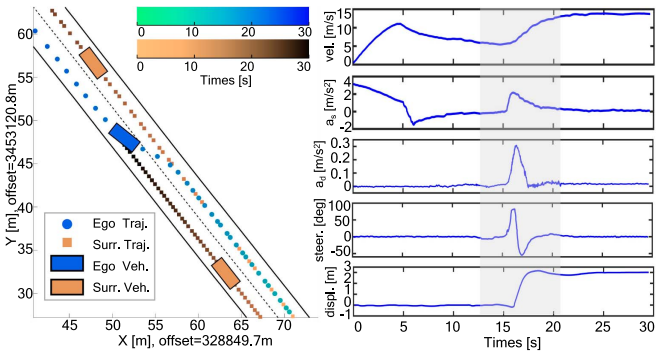

Fig. 15. (a) Vehicle trajectory visualization. (b) Results of real-world test, shown from top to bottom, illustrate the EV's velocity, longitudinal acceleration a_{s}, lateral acceleration a_{d}, steering wheel angle, and lateral displacement during the overtaking process over time.

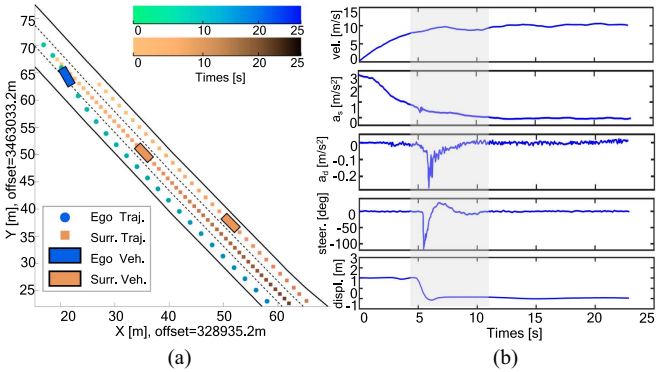

Fig. 16. (a) Vehicle trajectory visualization. (b) Results of real-world test, shown from top to bottom, illustrate the EV's velocity, longitudinal acceleration a_{s}, lateral acceleration a_{d}, steering wheel angle, and lateral displacement during the overtaking process over time.

5 s, then decelerates while following SV1 and waiting for a suitable overtaking opportunity. Once the gap between SV1 and SV2 is sufficient for a safe overtaking (around 16 s), the EV promptly initiates the lane change and accelerates to overtake SV1. These results verify that the EV can successfully complete the lane change and overtaking maneuvers when there are other slow SVs interfering.

B. Case 2: Three-Lane Overtaking Scenario

Case 2 involves a three-lane curved road. The EV starts in the middle lane with an initial velocity of 0 km/h, then gradually accelerates to 36 km/h. SV1 is 30 m ahead of the EV in the longitudinal direction, traveling at 15 km/h in the left lane. SV2 is in the same lane as the EV, 20 meters ahead, traveling at 12 km/h. The designed scenario is shown in Fig. 14(b). The trajectories of the EV and SVs are shown in Fig. 16(a). Considering the risk zone of the surrounding vehicles, even though SV2 is faster and has more space behind it, the repulsive forces of both SVs will still cause the EV to change lanes and overtake in the lane without obstacles, thereby avoiding unnecessary lane changes.

VII. Conclusion

In this article, a motion planning framework based on hybrid model predictive control is proposed to achieve seamless overtaking maneuvers. By integrating discrete logic decision-making and continuous motion planning in a single optimal problem, the approach enables more fluid and adaptable motion planning while still supporting extended access to semantic decisions. A novel asymmetric risk field considering human driver's attention feature is also incorporated into intrinsic discrete behavior optimization. Comprehensive validation is performed, including MATLAB simulation, nuPlan benchmark, and cloud-controlled real-world tests. The results demonstrate our algorithm's capability to identify overtuning opportunities, improve driving efficiency and safety, and showcase its potential for integrating decision-making, trajectory planning, and motion control in real autonomous driving tasks through an optimization scheme. Future work includes further investigating long-term performance and addressing prediction uncertainty caused by measurements to account for more complex scenarios.

Appendix
Conversion of Logical Constraints

In this section, we illustrate the details of transforming (24) into mixed integer inequalities. To represent the logical relations $[\Delta l_j(k)=0]$ with Boolean variables, introduce auxiliary variables $\delta_{j,k}$ to make

$$\underbrace{[\Delta l_j(k)\le 0]}_{(A_1)} \wedge \underbrace{[\Delta l_j(k)\ge 0]}_{(A_2)} \Leftrightarrow \underbrace{[\delta_{j,k}=1]}_{(A_3)}. \tag{A.1}$$

Then, transform the (A.1) into mixed integer inequalities

$$(A_1):\begin{cases} M\delta_{j1,k}\le M-\Delta l_j(k) \\ (\varepsilon-m)\delta_{j1,k}\ge \varepsilon-\Delta l_j(k). \end{cases} \tag{A.2a}$$

$$(A_2):\begin{cases} -m\delta_{j2,k}\le \Delta l_j(k)-m \\ (M+\varepsilon)\delta_{j2,k}\ge \Delta l_j(k)+\varepsilon. \end{cases} \tag{A.2b}$$

$$(A_3):\begin{cases} -\delta_{j1,k}+\delta_{j3,k}\le 0 \\ -\delta_{j2,k}+\delta_{j3,k}\le 0 \\ \delta_{j1,k}+\delta_{j2,k}-\delta_{j3,k}\le 1. \end{cases} \tag{A.2c}$$

Similarly, the remaining part of (24) is transformed in the same way

$$(B):\begin{cases} -m\delta_{j4,k}\le d_j(k)-m \\ (M+\varepsilon)\delta_{j4,k}\ge d_j(k)+\varepsilon. \end{cases} \tag{A.3a}$$

$$(A\wedge B):\begin{cases} -\delta_{j3,k}+\delta_{j5,k}\le 0 \\ -\delta_{j4,k}+\delta_{j5,k}\le 0 \\ \delta_{j3,k}+\delta_{j4,k}-\delta_{j5,k}\le 1 \end{cases} \tag{A.3b}$$

Then, $[|d_j(k)|\ge d_{safe}]$ can be rewritten as

$$\delta_{j5,k}(d_j(k)-d_{safe})\ge 0 \tag{A.4}$$

which is a nonlinear constraint, we can define new auxiliary real variables $\delta_{j6,k}=\delta_{j5,k}d_j$, subject to

$$\begin{cases} d_{\min}\delta_{j5,k}\le \delta_{j6,k}\le d_{\max}\delta_{j5,k} \\ -d_{\max}(1-\delta_{j5,k})\le \delta_{j6,k}-d_j\le -d_{\min}(1-\delta_{j5,k}). \end{cases} \tag{A.5}$$

Finally, we can obtain linear safety constraint

$$\delta_{j6,k} d_j(k) - \delta_{j5,k} d_{safe} \geq 0. \tag{A.6}$$

REFERENCES

[1] B. Leng et al., "Multi-mode evasion assistance control method for intelligent distributed-drive electric vehicle considering human driver's reaction," *Chin. J. Mech. Eng.*, vol. 38, no. 1, 2025, Art. no. 102.

[2] Y. Liu, A. Zhou, Y. Wang, and S. Peeta, "Proactive longitudinal control to assist lane changes of human-driven vehicles in mixed traffic: Human-emulation approach," *Automot. Innov.*, pp. 1–17, 2025.

[3] V. Z. Patterson, *An Architecture for Integrated Decision-Making, Motion Planning, and Control of Automated Vehicles.* Stanford, CA, USA: Stanford Univ. Press, 2022.

[4] T. Zhang, M. Fu, and W. Song, "Risk-aware decision-making and planning using prediction-guided strategy tree for the uncontrolled intersections," *IEEE Trans. Intell. Transp. Syst.*, vol. 24, no. 10, pp. 10791–10803, Oct. 2023.

[5] C. R. Baker and J. M. Dolan, "Traffic interaction in the urban challenge: Putting boss on its best behavior," in *Proc. IEEE Int. Conf. Intell. Rob. Syst.*, 2008, pp. 1752–1758.

[6] Z. Li, J. Hu, B. Leng, L. Xiong, and Z. Fu, "An integrated of decision making and motion planning framework for enhanced oscillation-free capability," *IEEE Trans. Intell. Transp. Syst.*, vol. 25, no. 6, pp. 5718–5732, Jun. 2024.

[7] P. Hang, C. Huang, Z. Hu, and C. Lv, "Driving conflict resolution of autonomous vehicles at unsignalized intersections: A differential game approach," *IEEE/ASME Trans. Mechatron.*, vol. 27, no. 6, pp. 5136–5146, Dec. 2022.

[8] M. Reda, A. Onsy, A. Y. Haikal, and A. Ghanbari, "Path planning algorithms in the autonomous driving system: A comprehensive review," *Robot. Autom. Syst.*, vol. 174, 2024, Art. no. 104630.

[9] G. Huang and Q. Ma, "Research on path planning algorithm of autonomous vehicles based on improved RRT algorithm," *Int. J. Intell. Transp. Syst. Res.*, vol. 20, pp. 170–180, 2022.

[10] J. Ziegler, M. Werling, and J. Schroder, "Navigating car-like robots in unstructured environments using an obstacle sensitive cost function," in *Proc. IEEE Intell. Veh. Symp.*, 2008, pp. 787–791.

[11] A. Puente-Castro, D. Rivero, A. Pazos, and E. Fernandez-Blanco, "A review of artificial intelligence applied to path planning in UAV swarms," *Neural Comput. Appl.*, vol. 34, no. 1, pp. 153–170, 2022.

[12] Y. Jiang, Z. Liu, D. Qian, H. Zuo, W. He, and J. Wang, "Robust online path planning for autonomous vehicle using sequential quadratic programming," in *Proc. IEEE Intell. Veh. Symp.*, 2022, pp. 175–182.

[13] Z. Q9in, L. Chen, M. Hu, and X. Chen, "A lateral and longitudinal dynamics control framework of autonomous vehicles based on multi-parameter joint estimation," *IEEE Trans. Veh. Technol.*, vol. 71, no. 6, pp. 5837–5852, Jun. 2022.

[14] H. Zhao, H. Yang, Y. Xia, and Z. Zuo, "Nonlinear terminal-free MPC on multitype bend tracking with discontinuous reference paths for autonomous vehicles," *IEEE Trans. Ind. Electron.*, vol. 71, no. 1, pp. 810–821, Jan. 2024.

[15] H. Li, C. Wu, D. Chu, L. Lu, and K. Cheng, "Combined trajectory planning and tracking for autonomous vehicle considering driving styles," *IEEE Access*, vol. 9, pp. 9453–9463, 2021.

[16] Z. Zuo et al., "MPC-based cooperative control strategy of path planning and trajectory tracking for intelligent vehicles," *IEEE Trans. Intell. Veh.*, vol. 6, no. 3, pp. 513–522, Sep. 2021.

[17] P. Hang, C. Lv, C. Huang, J. Cai, Z. Hu, and Y. Xing, "An integrated framework of decision making and motion planning for autonomous vehicles considering social behaviors," *IEEE Trans. Veh. Technol.*, vol. 69, no. 12, pp. 14458–14469, Dec. 2020.

[18] Z. Li et al., "A survey of reinforcement learning-based motion planning for autonomous driving: Lessons learned from a driving task perspective," 2025, *arXiv:2503.23650*.

[19] P. Wu, X. Jia, L. Chen, J. Yan, H. Li, and Y. Qiao, "Trajectory-guided control prediction for end-to-end autonomous driving: A simple yet strong baseline," in *Proc. Adv. Neural Inf. Process. Syst.*, Red Hook, NY, USA: Curran Associates Inc., 2022.

[20] D. Song, B. Zhu, J. Zhao, and J. Han, "Human–machine shared lateral control strategy for intelligent vehicles based on human driver risk perception reliability," *Automot. Innov.*, vol. 7, no. 1, pp. 102–120, 2024.

[21] P. Lin and M. Tsukada, "Model predictive path-planning controller with potential function for emergency collision avoidance on highway driving," *IEEE J. Robot. Autom.*, vol. 7, no. 2, pp. 4662–4669, Apr. 2022.

[22] Z. Zuo, X. Yang, Z. Zhang, and Y. Wang, "Lane-associated MPC path planning for autonomous vehicles," in *Proc. Chin. Control Conf. (CCC)*, 2019, pp. 6627–6632.

[23] U. Z. Abdul Hamid, H. Zamzuri, T. Yamada, M. A. Abdul Rahman, Y. Saito, and P. Raksincharoensak, "Modular design of artificial potential field and nonlinear model predictive control for a vehicle collision avoidance system with move blocking strategy," in *Proc. Inst. Mech. Eng., Part D, J. Automobile Eng.*, vol. 232, no. 10, pp. 1353–1373, 2018.

[24] C. Tu, Z. Li, B. Leng, and L. Xiong, "A seamless motion planning integrating maneuver decision based on hybrid model predictive control," in *Proc. IEEE 26th Int. Conf. Intell. Transp. Syst. (ITSC),* 2023, pp. 3228–3234.

[25] A. Bemporad and V. V. Naik, "A numerically robust mixed-integer quadratic programming solver for embedded hybrid model predictive control," *IFAC-PapersOnLine*, vol. 51, no. 20, pp. 412–417, 2018, 6th IFAC Conference on Nonlinear Model Predictive Control NMPC 2018.

[26] W. L. Winston, M. Venkataramanan, and J. B. Goldberg, *Introduction to Mathematical Programming.* vol. 1., Pacific Grove, CA, USA: Thomson/Brooks/Cole Duxbury, 2003.

[27] Y. B. Eisma, D. J. Eijssen, and J. C. de Winter, "What attracts the driver's eye? Attention as a function of task and events," *Information*, vol. 13, no. 7, 2022, Art. no. 333.

[28] M. Witt, L. Wang, F. Fahrenkrog, K. Kompaß, and G. Prokop, "Cognitive driver behavior modeling: Influence of personality and driver characteristics on driver behavior," in *Proc. Adv. Human Aspects Transportation*, New York, NY, USA: Springer, 2019, pp. 751–763.

[29] P. Polack, F. Altché, B. D, A. Novel, and A. de La Fortelle, "The kinematic bicycle model: A consistent model for planning feasible trajectories for autonomous vehicles?" in *Proc. IEEE Intell. Veh. Symp.*, 2017, pp. 812–818.

[30] S. A. of China (SAC), "*Motor vehicles - devices for indirect vision - requirements of performance and installation*," GB 15084-2022, 2022.

[31] N. Karnchanachari et al., "Towards learning-based planning: The nuPlan benchmark for real-world autonomous driving," in *Proc. IEEE Int. Conf. Robot. Autom. (ICRA)*, Piscataway, NJ, USA: IEEE Press, 2024, pp. 629–636.

[32] J. Cheng, Y. Chen, X. Mei, B. Yang, B. Li, and M. Liu, "Rethinking imitation-based planners for autonomous driving," in *Proc. IEEE Int. Conf. Robot. Autom. (ICRA)*, Piscataway, NJ, USA: IEEE Press, 2024, pp. 14123–14130.

[33] D. Dauner, M. Hallgarten, A. Geiger, and K. Chitta, "Parting with misconceptions about learning-based vehicle motion planning," in *Proc. Conf. Robot Learn.*, PMLR, 2023, pp. 1268–1281.

[34] X. Zhang, L. Xiong, P. Zhang, J. Huang, and Y. Ma, "Real-world troublemaker: A 5G cloud-controlled track testing framework for automated driving systems in safety-critical interaction scenarios," *IEEE Internet Things J.*, vol. 12, no. 23, pp. 50617–50631, Dec. 2025.

Bo Leng (Member, IEEE) received the Ph.D. degree in vehicle engineering from Tongji University, Shanghai, China.

He is currently working as an Associate Professor with the School of Automotive Studies, Tongji University. His research interests include dynamic control of distributed drive electric vehicles, and motion planning and control of intelligent vehicles.

Dr. Leng has won the first prize of China Automobile Industry Technology Invention Award, the First Prize of Shanghai Science and Technology Progress Awards in 2020 and 2022, respectively. He has been selected into the Young Elite Scientists Sponsorship Program of China Association for Science and Technology in 2022.

Ran Yu received the B.S. degree in vehicle engineering from the School of Automotive Engineering, Harbin Institute of Technology, Weihai, China, in 2024. He is currently working toward the M.S. degree in vehicle engineering from the School of Automotive Studies, Tongji University, Shanghai, China.

His research interests include safe reinforcement learning, and motion planning and control of intelligent vehicles.

Chengen Tu received the B.S. degree in mechanical engineering from the School of Mechanical Engineering, Xi'an Jiaotong University, Xi'an, China, in 2021. He is currently working toward the M.S. degree in vehicle engineering from the School of Automotive Studies, Tongji University, Shanghai, China.

His research interests include motion planning and model predictive control.

Lu Xiong received the Ph.D. degree in vehicle engineering from Tongji University, Shanghai, China, in 2005.

He is currently the Vice President and a Professor with the School of Automotive Studies, Tongji University. His research interests include dynamic control of distributed drive electric vehicles, motion planning and control of intelligent vehicles, and all-terrain vehicles.

Dr. Xiong has won the First Prize of Shanghai Science and Technology Progress Awards in 2013, 2020 and 2022. He was the recipient of the National Science Fund for Distinguished Young Scholars.

Arno Eichberger (Member, IEEE) received the M.Sc. degree in mechanical engineering and the Ph.D. degree (Hons.) in technical sciences from Graz University of Technology, Graz, Austria, in 1995 and 1998, respectively.

From 1998 to 2007, he was employed with Magna Steyr Fahrzeugtechnik AG & Company, Graz, where he dealt with different aspects of active and passive safety. Since 2007, he has been with the Institute of Automotive Engineering, Graz University of Technology, dealing with driver assistance systems, vehicle dynamics, and suspensions. Since 2012, he has been an Associate Professor holding a "venia docendi" of automotive engineering. He is currently the Director of Institute of Automotive Engineering.

Zhuoren Li (Member, IEEE) received the B.E. degree in engineering mechanics and the Ph.D. degree in vehicle engineering from Tongji University, Shanghai, China, in 2019 and 2025, respectively.

His research interests include safe reinforcement learning, large language model enhanced end-to-end autonomous driving, interaction decision-making, and motion planning of autonomous vehicles.